Investigation of the Relationship Between Tracking Accuracy and Tracking Distance of a Novel Magnetic Tracking System

Shijian Su, Wanan Yang, Houde Dai, Xuke Xia, Mingqiang Lin, Bo Sun, and Chao Hu

***Abstract*— The position and orientation of an object embedding with a permanent magnet can be acquired in real time via a magnetic tracking system. However, one characteristic of the magnetic tracking technique is its varied tracking accuracy along with the tracking distance. Hence, this paper tends to investigate the relationship between the tracking accuracy and the distance from the magnet to the sensor array by both simulations and experiments. Results show that the relationship is expressed as a cubic polynomial equation, and that the equation coefficients are related to the properties of the magnet and the signal-to-noise ratio of the sensor outputs. When the magnet is located at a distance from 36 to 96 mm above the sensor array, the system had the best performance, while average localization and orientation errors were 0.70 mm and 1.22°, respectively. Thus, this system achieved the best tracking accuracy compared with the state-of-the-art of magnetic tracking systems. This paper is helpful to the researchers who want to implement a magnetic tracking system or need to know clearly the valid tracking distance of a magnetic tracking system.**

***Index Terms*— Localization and orientation, digital-output magnetic sensor, real-time tracking, magnetic tracking system.**

I. Introduction

IN THE industrial field, automated guided vehicle (AGV) can move and stop precisely based on the magnetic localization [1], [2]. Due to the use of line magnetic sensor array, the positioning accuracy is about 3.25mm [3]. In the medical field, wireless capsule endoscopy (WCE) offers a noninvasive and painless investigation for the entire gastrointestinal track [4]. However, the practical tracking system for WCE during the diagnostic inspection of the gastrointestinal track has not been reported at present. Tracking WCE can provide doctors with the positions of each endoscopic image. At the same time, the position and orientation of the capsule can also be used for its feedback control [5]–[7]. The magnetic tracking system can be classified into two types according to the magnetic field excitation source: permanent magnet tracking and quasi-static magnetic coils tracking [16]–[19]. Generally, the intensity and direction of the magnetic field excited by the target source are related to its position and orientation. Magnetic sensors can be used to measure the magnetic fields; thus the position and orientation of the target embedded with the magnet can be evaluated via appropriate algorithms. The permanent magnet has the characteristic of power-free, and it has the prospect to be applied in different applications.

In the last decade, many researchers conducted their research on permanent magnet tracking [8]–[15]. For instance, Schlageter *et al.* developed a 5DOF (degree-of-freedom) tracking system based on a 2D (two-dimensional)-array of 16 hall sensors and a magnet of 0.2cm^3 [8], [9]. In the experiment, its detection distance was up to 200mm, but its tracking accuracy did not present itself. Son *et al.* developed a magnetic localization setup for an untethered meso-scale magnetic robot [6]. The resulting position error was 2.1mm and angular error was 6.7° within the applicable range (50mm). Sherman *et al.* also developed a system using a planar array of 27 magnetic sensors [11]. The position and orientation of a magnet (Ø4.55×6.35mm, remanence $Br = 1.31 \pm 0.01$T) were determined, while maximum errors were3.8mm and 4.2° respectively. Song *et al.* [20] presented a sensor layout strategy and built a magnetic localization system based on the layout optimization results of the whole domain. The average localization and orientation errors were 1.4mm and 3.4° respectively.

In previous studies, we have developed a series of magnetic tracking systems. Anisotropic magneto-resistive (AMR) sensors such as Honeywell HMC1053 and HMC1043 were adopted. The average localization and orientation errors were about 3.3mm and 3.0° based on a 2D HMC1053 sensor array [21], [22].

To improve the accuracy and to enlarge the localization space, a cubic sensor array based on HMC1043 was designed, as shown in Fig. 1 [14]. The system achieved an average position error of 1.8mm and orientation error of 1.6°. This system has good performance in localization accuracy and response time. However, each sensor was soldered on a separated PCB

Manuscript received May 18, 2017; revised June 4, 2017; accepted June 5, 2017. Date of publication June 8, 2017; date of current version July 10, 2017. This work was supported in part by the National Natural Science Foundation of China under Grant 61501428 and Grant 61273332, in part by the Chinese Academy of Sciences under Project YZ201510 (Research Equipment Development Project of the Chinese Academy of Sciences), in part by Ningbo Science and Technology (Innovation Team) plan Project under Grant 2014B82015, and in part by Quanzhou Science and Technology Project under Grant 2015G130, Grant 2016G006, and Grant 2016G044. The associate editor coordinating the review of this paper and approving it for publication was Dr. Jürgen Kosel. *(Corresponding authors: Houde Dai; Mingqiang Lin.)*

S. Su, H. Dai, X. Xia, M. Lin, and B. Sun are with the Quanzhou Institute of Equipment Manufacturing, Haixi Institutes, Chinese Academy of Sciences, Jinjing, Fujian 362200, China (e-mail: dhd@fjirsm.ac.cn; kdlmq@fjirsm.ac.cn).

W. Yang is with the School of Computer and Information Engineering, Yibin University, China (e-mail: ywaly@126.com).

C. Hu is with the Ningbo Institute of Technology, Zhejiang University, Ningbo 315000, China (e-mail: huchao@nit.net.cn).

Digital Object Identifier 10.1109/JSEN.2017.2713886

Fig. 1. Cubic magnetic tracking system. Left: cubic sensor array; Right: signal processing and control circuits.

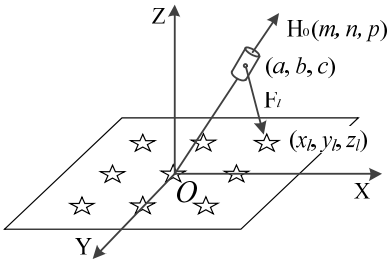

Fig. 2. Magnetic dipole model for this tracking system. The permanent magnet is modeled as a magnetic dipole with the position parameters (a, b, c) and orientation parameters (m, n, p). The magnetic field intensity at the l-th sensor is $\mathbf{B_l}$, while the position of the sensor is (x_l, y_l, z_l), $1 \leq l \leq$N.

(printed circuit board) and connected each other via wires. Hence, its complex cables and circuit boards can easily lead to poor contact. What is more, the previous systems presented the average accuracy during the whole space above the sensor array. In fact, the tracking accuracy varied with the distance from the magnet to the sensor array. The relationship between the tracking accuracy and the distance from the magnet to the sensor array is not clear until now. However, this relationship is of importance when designing the cubic sensor array in actual applications.

This paper extends our previous study by:

1) implementing a new planar sensor array based on nine tri-axis digital magnetic sensors and a single PCB to simplify the hardware structure and to reduce the power consumption. Thus, it has higher application potential;
2) exploring the relationship between the localization accuracy and the distance from the magnet to the sensor array. It is necessary to consider the relationship when implementing a magnetic tracking system.

The paper is organized as follows. Section II presents the localization model and algorithms. Section III depicts the prototype implementation. An improved calibration method for the sensor array and the tracking accuracy evaluation of this system are introduced in Section IV. Section V presents the accuracy-versus-distance evaluation of the magnetic tracking system, which is followed by the conclusions in Section VI.

II. Mathematical Model and Algorithms

A. Mathematical Model

The magnetic field intensity of the cylindrical magnet can be represented by a dipole model because the magnet's pose parameters based on dipole model are reliable compared with the quadrupole extension model [12].

As shown in Fig. 2, (a, b, c) is the center of the magnet, and (x_l, y_l, z_l) is the position of the l-th sensor. $\mathbf{H}_0$ is a unit vector $(m, n, p)^T$ representing the magnet's orientation from south pole to north pole. $\mathbf{F}_l$ denotes the vector from (a, b, c) to (x_l, y_l, z_l). The magnetic field intensity $\mathbf{B_l}$ at point (x_l, y_l, z_l) can be expressed as:

$$\begin{aligned}\mathbf{B}_l &= B_{lx}i + B_{ly}j + B_{lz}k \\ &= B_T\left(\frac{3(\mathbf{H}_0 \cdot \mathbf{F}_l)\mathbf{F}_l}{R_l^5} - \frac{\mathbf{H}_0}{R_l^3}\right)(l = 1, 2, \ldots, N), \end{aligned} \quad (1)$$

where N is the total number of the sensors; B_T is a constant related to the magnet [14], and is defined as:

$$B_T = \frac{\mu_r \mu_0 \pi \delta^2 L M_0}{4\pi}, \quad (2)$$

where μ_r is the relative permeability of the medium (in the air, $\mu_r \approx 1$); μ_0 is the air magnetic permeability ($\mu_0 = 4\pi \cdot 10^{-7}\mathrm{T \cdot m/A}$); δ and L denote the radius and length of the cylindrical magnet respectively; M_0 (unit: A/m) represents the magnetization on the surface of the magnet.

B. Localization Algorithms

Two or more tri-axis magnetic sensors can be used to measure the magnetic field intensity around a magnet. Using the measured data and the mathematical model (1), the magnet's position and orientation parameters can be computed with an appropriate nonlinear optimization algorithm. Extending (1), we have

$$B_{lx} = B_T\{\frac{3[m(x_l-a)+n(y_l-b)+p(z_l-c)]\cdot(x_l-a)}{R_l^5} - \frac{m}{R_l^3}\}, \quad (3)$$

$$B_{ly} = B_T\{\frac{3[m(x_l-a)+n(y_l-b)+p(z_l-c)]\cdot(y_l-b)}{R_l^5} - \frac{n}{R_l^3}\}, \quad (4)$$

$$B_{lz} = B_T\{\frac{3[m(x_l-a)+n(y_l-b)+p(z_l-c)]\cdot(z_l-c)}{R_l^5} - \frac{p}{R_l^3}\}, \quad (5)$$

where B_{lx}, B_{ly}, and B_{lz} are the three components of the magnetic field intensity along X, Y, and Z axes.

Supposing $(B_{lx}, B_{ly}, B_{lz})^T$ and $(B'_{lx}, B'_{ly}, B'_{lz})^T$ are the theoretical values and measured values by the sensors, the error objective function can be defined as:

$$E = \sum_{l=1}^{N}(B_{lx} - B'_{lx})^2 + \sum_{l=1}^{N}\left(B_{ly} - B'_{ly}\right)^2 + \sum_{l=1}^{N}(B_{lz} - B'_{lz})^2. \quad (6)$$

There are several algorithms to search for the optimal solution of (6), such as Levenberg-Marquard (LM), Powell, and DIRECT algorithms [7]–[18]. Considering the real-time performance and accuracy, the LM algorithm was selected [23]. The LM algorithm needs an initial guess value in the iteration process. If the initial guess value is far from the true value,

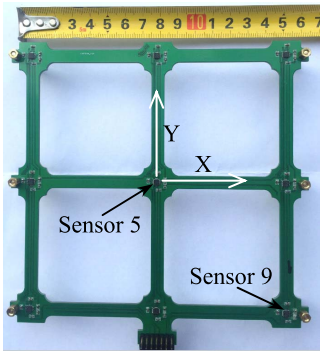

Fig. 3. Planar array was based on nine digital magnetic sensors and a single PCB. All sensors are arranged in the same X-Y plane. Nine sensors were evenly organized in a horizontal plan.

the algorithm will be easy to converge to the local optimal solution. Furthermore, it is difficult to determine the initial guess in the practical application.

The particle swarm optimization (PSO) algorithm has the advantage of no initial guess value in need. To ensure the convergence and to keep the diversity of the particles, the hybrid strategy of PSO and Clone algorithm was adopted [24].

Firstly, the hybrid algorithm was repeatedly performed to search the solutions for three times independently. After that, the best one, i.e. the minimum of the fitness values, is chosen as the initial guess value of the LM algorithm. Hence, the output of the LM algorithm is taken as the first point of the magnet's locus. In the subsequent tracking process, the last point computed by the LM algorithm is regarded as the initial guess value of the LM algorithm in the next computation. The result of the computation is taken as the new point of the magnet's locus.

If the permanent magnet rotates around itself, i.e. its center $\mathbf{H}_0$, $\mathbf{B}_l$ has no change; thus, this magnetic tracking system performs 3D localization and 2D orientation.

III. Prototype Implementation

A. A. Planar Sensor Array

Magnetic sensors play an important role in improving the performance of the magnetic tracking system. To guarantee the performance, it is essential for the sensors to be of high sensitivity, wide range and strong anti-interference ability.

To reduce complexity and power consumption, analog magnetic sensors were replaced by digital magnetic sensors. The amplifier, multiplexer, and analog-to-digital converter are integrated inside the digital sensor. In addition, full-scale range settings and programmable filters are available inside each digital sensor.

Magnetic sensor LSM303D (STMicroelectronics Inc., Switzerland) was adopted in the tracking system. The full scale of LSM303D was set as $\pm$400uT and its resolution is 0.016uT.

Fig. 3 shows the planar sensor array composed of nine LSM303D units which were soldered to a single PCB with the dimension of $150 \times 150\text{mm}^2$. The structure is simplified and its reliability is improved. The reason why using a single plane for the sensor array is to investigate the relationship between the localization accuracy and the distance from the magnet to the sensor array. The dimension of the sensor array can be increased or decreased according to the application fields in the future.

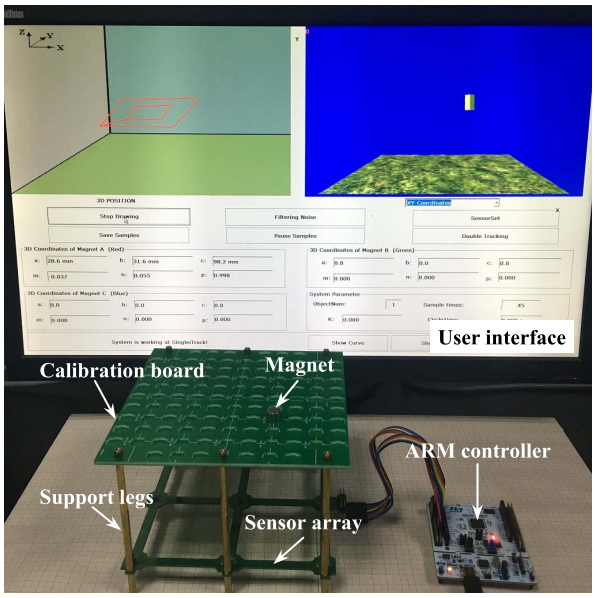

Fig. 4. Prototype of the magnetic tracking system. The Nd-Fe-B magnet was tracked in real-time when it was placed above the sensor array. The position and orientation parameters were displayed in the graphical user interface. Operation buttons such as "Start tracking," "Calibrating," and "Drawing" could be clicked.

B. B. Prototype Implementation

As shown in Fig. 4, a novel prototype was built up in this study, including a digital-output magnetic sensor array, an ARM controller, a calibration board and a personal computer. The ARM controller STM32F103 (STMicroelectronics Inc., Switzerland) reads the magnetic sensor data via SPI (serial peripheral interface) bus and then transmits them to the computer via a USB (universal serial bus) to UART (universal asynchronous receiver/transmitter) interface. The computer executes the localization algorithm and displays the position, the orientation and movement locus of the magnet in real time.

The graphical user interface of the tracking system, which displays the 3D locus of the magnet at 20Hz data updating rate, is based on the Microsoft Visual C++2010 (Microsoft Inc., USA).

The power supply of the tracking system was 5V. Currents of the tracking system and the sensor array were measured with a $6^1/_2$ digital multimeter (Keysight 34410A, Keysight Technologies, Inc., USA). Measurement results show that the sensor array and ARM controller consumed about 455mW totally, while the sensor array consumed only 45mW.

IV. Calibration of the Sensor Array and Tracking Accuracy Evaluation

To improve the accuracy of the tracking system, the calibration of each sensor is indispensable. The calibration method for analog magnetic sensor had been illustrated

in [25], whereas the calibration of digital sensors have some differences.

When calibrating analog magnetic sensors, the cylindrical magnet was placed at the intersection point of horizontal and vertical mark manually, and the bottom center of the magnet may not overlap with the intersection point [25]. As shown in Fig. 4, a novel two-layer calibration board, with the same dimension of the planar sensor array (i.e., $150\times150\text{mm}^{2)}$ was designed. The thickness of the bottom layer was 1.0mm. The top layer of the calibration board was marked with high-precision scale lines and carved evenly with 121 holes. The holes had the same dimension (i.e., $\emptyset10\times10$mm) and can just locate a permanent magnet. The machining accuracy of the calibration board was better than 0.01mm.

The magnet was put at the specific locations on the calibration board when the distance between the calibration board and the sensor array was 76mm. The locations and orientations of the magnet and the outputs of the sensors were recorded. In the following calibration process, we just illustrated the calibration for the l-th sensor, and other sensors were calibrated by using the same method.

A. Determining B_T

The output of the analog magnetic sensor is not the value of the magnetic field intensity, and there is a factor between the output of the analog magnetic sensor and the magnetic field intensity. The value of the factor can be determined in the calibration [25]. However, the sensitivity of the digital magnetic sensor has been calibrated in the factory, and the output of the digital magnetic sensor is the magnetic field intensity. Hence, we need to modify the parameters of (1), instead of the sensitivity factors of magnetic sensors. As the parameter B_T of (1) is related to the magnetic properties, the unknown parameter B_T should be determined before the tracking process.

There are two methods to determine B_T. Firstly, it can be calculated according to (2). M_0 is 1.032×10^6A/m for the Nd-Fe-B magnet with the grade of N35. However, M_0 for each actual N35 magnet has small difference and μ_r varies during different air conditions. Secondly, it can be obtained by calibration. Supposing $B_{ix}^{'}$ is the output of the sensor's x-axis when the magnet is put at the i-th location, thus we define $\hat{B}_{ix}$ as follow:

$$\hat{B}_{ix}=\frac{3[m_i(x_l-a_i)+n_i(y_l-b_i)+p_i(z_l-c_i)]\cdot(x_l-a_i)}{R_i^5}-\frac{m_i}{R_i^3}. \tag{7}$$

Hence the error objective function is defined as:

$$E_{btx}=\sum_{i=1}^{D}(B'_{ix}-B_T\cdot\hat{B}_{ix})^2, \tag{8}$$

where D is the number of sampled data.

B_T can be calculated by the least square method. Using the same method, we can obtain B_T according to the output of y-axis and z-axis. Owing to the noises and measurement errors, each B_T from different axis will be slightly different. The average value of different B_T is regarded as the final B_T.

B. Sensor Position Calibration

There are deviations between the sensors' real positions and their predetermined positions in the sensor array. The deviations originate from the asymmetry of the cross-axis misalignment of each sensor and the inconformity of sensors when being welded on the printed circuit board.

Assume that $(B_{ix}^{'}, B_{iy}^{'}, B_{iz}^{'})^T$ is the sensor output when the magnet is put at the i-th location, then the error objective function can be defined as:

$$E_{sp}=\sum_{i=1}^{D}\left(B_{ix}-B'_{ix}\right)^2+\sum_{i=1}^{D}\left(B_{iy}-B'_{iy}\right)^2+\sum_{i=1}^{D}\left(B_{iz}-B'_{iz}\right)^2. \tag{9}$$

Minimizing the value of E_{sp}, the sensor position parameter (x_l, y_l, z_l) in $(B_{ix}, B_{iy}, B_{iz})^T$ is obtained by the LM algorithm.

C. Sensor Orientation Calibration

The three axes of each sensor might not be exactly parallel to the corresponding axes of the tracking system, which will affect the localization accuracy. We amended this error by vector transformation using the sampled data.

Assume that $(B_{ix}^{'}, B_{iy}^{'}, B_{iz}^{'})^T$ is the sensor output when the magnet is put at the i-th location, $(\tilde{B}_{ix}, \tilde{B}_{iy}, \tilde{B}_{iz})^T$ is the adjusted magnetic field intensity. The orientation adjustment can be described as:

$$\begin{bmatrix}\tilde{B}_{ix}\\ \tilde{B}_{iy}\\ \tilde{B}_{iz}\end{bmatrix}=\mathbf{O}\begin{bmatrix}B'_{ix}\\ B'_{iy}\\ B'_{iz}\end{bmatrix}=\begin{bmatrix}o_{11} & o_{12} & o_{13}\\ o_{21} & o_{22} & o_{23}\\ o_{31} & o_{32} & o_{33}\end{bmatrix}\begin{bmatrix}B'_{ix}\\ B'_{iy}\\ B'_{iz}\end{bmatrix}, \tag{10}$$

where $\mathbf{O}$ is the adjusting matrix. To solve the matrix $\mathbf{O}$, we define the error objective function as:

$$E_{so}=\sum_{i=1}^{D}(B_{ix}-\tilde{B}_{ix})^2+\sum_{i=1}^{D}(B_{iy}-\tilde{B}_{iy})^2+\sum_{i=1}^{D}(B_{iz}-\tilde{B}_{iz})^2, \tag{11}$$

where $(B_{ix}, B_{iy}, B_{iz})^T$ can be calculated by (4), (5), and (6) according to the predetermined position and orientation of the magnet. Minimizing the value of E_{so}, the matrix $\mathbf{O}$ can be obtained by using the least square method.

D. Tracking Accuracy Evaluation

Because there are some holes for holding the magnet on the calibration board, the magnet can be placed accurately in the predetermined position. The magnet was placed 50 times evenly on the calibration board whose distance are 66mm and 86mm respectively above the sensor array. The localization values and predetermined values of the magnet are shown in Fig. 5.

To investigate the localization and orientation accuracy, the position and orientation errors are defined as E_{pi} and E_{oi} respectively:

$$E_{pi}=\sqrt{(a_{ci}-a_{ri})^2+(b_{ci}-b_{ri})^2+(c_{ci}-c_{ri})^2}, \tag{12}$$

$$E_{oi}=\sqrt{(m_{ci}-m_{ri})^2+(n_{ci}-n_{ri})^2+(p_{ci}-p_{ri})^2}, \tag{13}$$

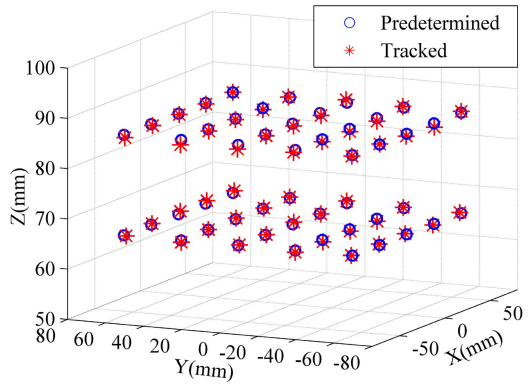

Fig. 5. 3D position plot for the true positions (i.e., predetermined positions) and the tracked positions by this magnetic tracking system. The magnet was placed in the holes of the calibration board when the distances from the magnet and sensor array were 66mm and 86mm, respectively.

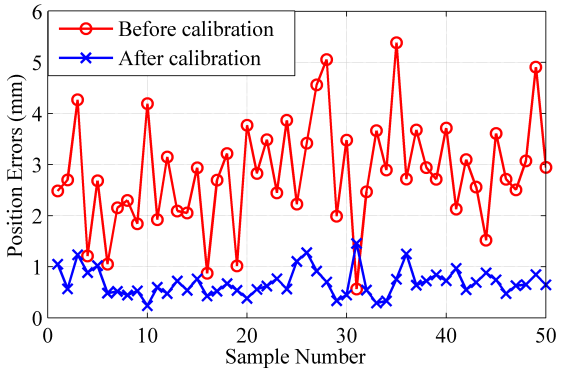

Fig. 6. Position errors before and after calibration (50 samples). In each sample point of the calibrated board, the position errors before and after calibration were recorded.

where $(a_{ri}, b_{ri}, c_{ri}, m_{ri}, n_{ri}, p_{ri})$ is the i-th predetermined value and $(a_{ci}, b_{ci}, c_{ci}, m_{ci}, n_{ci}, p_{ci})$ is the i-th localization value.

The orientation error can be converted to angle error using $2\sin^{-1}(E_{oi}/2)$. The root-mean-square (RMS) values of the total localization and orientation errors of N samples are described as:

$$E_{ptotal} = \sqrt{\frac{1}{N}\sum_{i=1}^{N}((a_{ci}-a_{ri})^2+(b_{ci}-b_{ri})^2+(c_{ci}-c_{ri})^2)}, \tag{14}$$

$$E_{ototal} = \sqrt{\frac{1}{N}\sum_{i=1}^{N}((m_{ci}-m_{ri})^2+(n_{ci}-n_{ri})^2+(p_{ci}-p_{ri})^2)}. \tag{15}$$

Similarly, $E_a, E_b, E_c, E_m, E_n, E_p$ in table I denote the RMS errors of each parameter of N samples.

Fig. 6 and Fig. 7 show the localization and orientation errors before and after calibration. It can be observed that the localization and orientation accuracies are improved greatly after the calibration. The localization errors of 86% samples were less than 1.0mm, and the orientation errors of 90% samples were less than 2°.

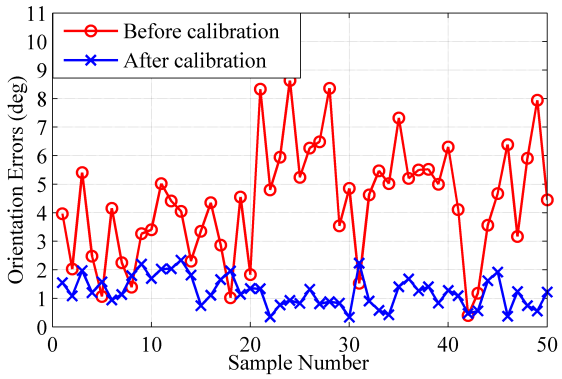

Fig. 7. Orientation errors before and after calibration (50 samples). In each sample point of the calibrated board, the orientation errors before and after calibration were recorded.

TABLE I
POSITION AND ORIENTATION ERRORS

	Before Calibration	***After Calibration***
E_a	2.23mm	0.42mm
E_b	1.50mm	0.48mm
E_c	1.39mm	0.38mm
E_{p_total}	3.02mm	0.74mm
E_m	0.0663(-)	0.0192(-)
E_n	0.0513(-)	0.0134(-)
E_p	0.0045(-)	0.0004(-)
E_{o_total}	4.81°	1.341°

Here E_a, E_b, and E_c denote the location errors in X-, Y- and Z-axis respectively; E_{p_total} means the summarized location error in X-Y-Z axes; E_m, E_n, and E_p denote the orientation errors of m, n, and p respectively; E_{o_total} represents the summarized orientation error.

Table I lists the detailed localization and orientation errors before and after calibration. The total localization error E_{ptotal} decreases from 3.02mm to 0.74mm, and the total orientation error E_{o_total} decreases from 4.81° to 1.34°.

E. Localization Stability Evaluation

The localization stability of the system was also evaluated. The permanent magnet was placed at the point (x = −30mm, y = 30mm, z = 96mm), and Fig. 8 shows the localization drifts during 3000 seconds. It can be seen that the variations of the position errors are within 1mm. The standard deviation of X-axis, Y-axis and Z-axis localization were 0.082mm, 0.086mm, and 0.046mm respectively.

V. ACCURACY-VERSUS-DISTANCE EVALUATION

In our previous studies, we found that the tracking accuracy varies with the distance between the sensor array and the magnet, whereas the tracking accuracy is stable when the magnet moves on a fixed plane in parallel with the sensor array. However, most of the available literature on magnetic tracking systems provided only the average tracking accuracy

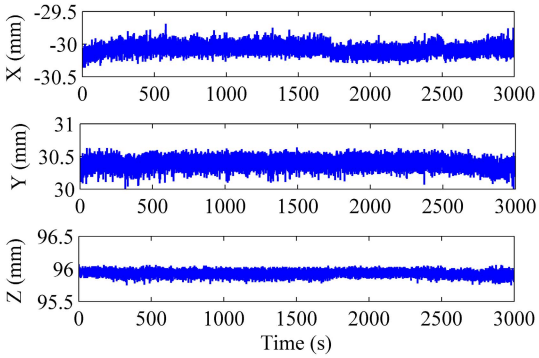

Fig. 8. Position drift (mm) during 3000 seconds.

in the whole tracking domain. Therefore, we investigated the relationship between the accuracy and the distance by both simulations and experiments.

In this study, an axially magnetized cylindrical Nd-Fe-B magnet (Ø10 × 10mm, remanence $Br = 1.22 \pm 0.01$T, $B_T = 8.1\times10^{-8}$T, grade: N35) was adopted in the experiment, while the earth field was 56.6uT and the average measured noise in each axis was ±0.2uT.

A. Simulation of the Magnetic Field Intensity Around a Permanent Magnet

One major disadvantage of a magnetic tracking system is that the tracking distance is limited. The reason is that the magnetic intensity around a magnet decreases rapidly. To investigate the magnetic intensity around a magnet in detail, the simulation of the magnetic induction intensity around a permanent magnet was performed.

According to (1), the distance R_l from the l-th sensor (x_l, y_l, z_l) to the magnet (a, b, c) can be acquired:

$$\mathbf{B}_l = \frac{B_T}{R_l^3}\left(\frac{3(\mathbf{H}_0 \cdot \mathbf{F}_l)\mathbf{F}_l}{R_l^2} - \mathbf{H}_0\right)(l = 1, 2, \ldots, N), \quad (16)$$

where $\mathbf{H}_0 = (m, n, p)^T$ representing the magnet's magnetic direction in the coordinate system of the sensor array; $R_l = \sqrt{(x_l - a)^2 + (y_l - b)^2 + (z_l - c)^2}$; and $\mathbf{F}_l = (x_l - a, y_l - b, z_l - c)$. According to Fig. 3, $\mathbf{H}_0$ and $\mathbf{F}_l$ equal (0, 0, 1) and (0, 0, c) respectively when the magnet's magnetic direction coincides with the Z-axis of the tracking system's coordinate. For the 5th sensor in Fig. 3, $R_5 = c$. Thus, $\mathbf{B}_5 = (B_{5x}, B_{5y}, B_{5z})$ can be modified as:

$$B_5 = \frac{B_T}{c^3}\left\{\frac{3[(0, 0, 1)\cdot(0, 0, c)]\times(0, 0, c)}{c^2} - (0, 0, 1)\right\}, \quad (17)$$

where $B_{5x} = B_{5y} = 0$. Thus, B_{5z} in the positive direction can be further simplified as:

$$B_{5z} = 2B_T/c^3. \quad (18)$$

Fig. 9 shows the relationship between the magnetic induction intensity at the 5th sensor of the sensor array and the distance from the magnet.

For the magnetic tracking algorithm implementation, at least two triaxial magnetic sensors are needed. Except for the 5th sensor, other sensors in the sensor array have even small

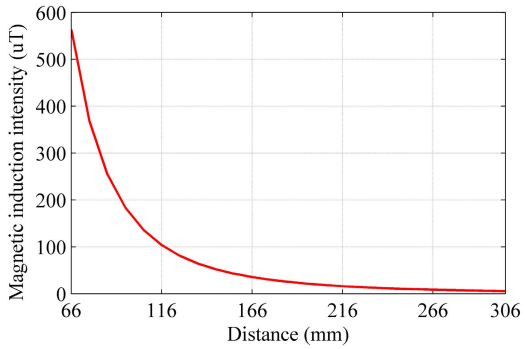

Fig. 9. Relationship between the magnetic induction intensity at the 5th sensor of the sensor array and the distance from the magnet. When the magnet was placed with the opposite magnetization direction ($\mathbf{H}_0$), the magnetic induction intensity was negative. Because the full scale of magnetic sensors was set at ±400uT in this study, we set the beginning of the distance at 66mm, where B_{5z} equals 564uT.

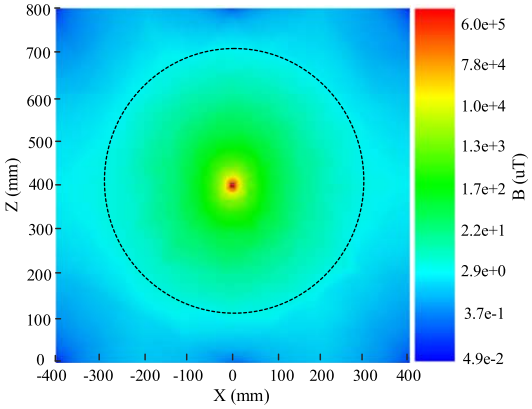

Fig. 10. XZ-plane slice view of the magnetic induction intensity of an axially magnetized cylindrical Nd-Fe-B magnet (Ø10 × 10mm, $Br = 1.22 \pm 0.01$T, $B_T = 8.1 \times 10^{-8}$T, grade: N35).

$\mathbf{B}_l$ when the magnet is placed in the top center of the sensor array.

The magnetic induction intensity around the magnet was also analyzed via the finite element software (Ansoft Maxwell 16.0, ANSYS Inc., USA). Fig. 10 shows the XZ-plane magnetic induction intensity around the magnet.

As shown in Fig. 9 and Fig. 10, the magnetic induction intensity becomes feeble (≈2.9uT) when the distance from the magnet center is beyond 300mm. However, the sensor noise at each point is almost the same (±0.2uT). The rapid attenuation of the magnetic field intensity means that the valid tracking range is limited. Comparing with Fig. 10, the tracking error has a more drastic increase along with the distance from the magnet to the sensor array. Thus, the distance during the accuracy-versus-distance experiment was set from 0 to 300mm.

B. Accuracy-Versus-Distance Experiments and Simulations

As Fig. 4 shows, a calibration board was adopted to place the permanent magnet, while its height above the sensor array was changed with the adjustable support legs.

During the experiment, we measured 25 points evenly in the calibration board for each varied distance, i.e. at 10mm interval from 16mm to 306mm for the distance between the magnet

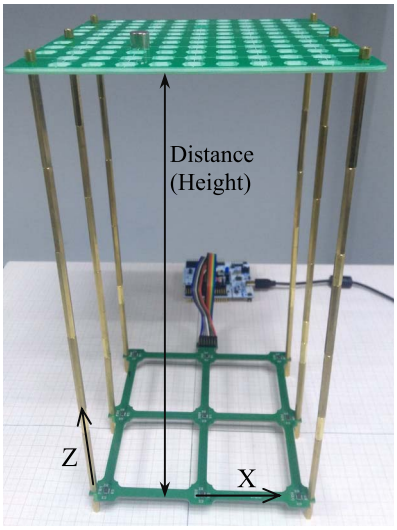

Fig. 11. Plot of the tracking system when the height of the magnet was 306mm. Dimensions of the sensor array and the calibration board were the same, while the adjustable support legs were perpendicular to both the sensor array and the calibration board. The grade of the adopted Nd-Fe-B magnet was N35.

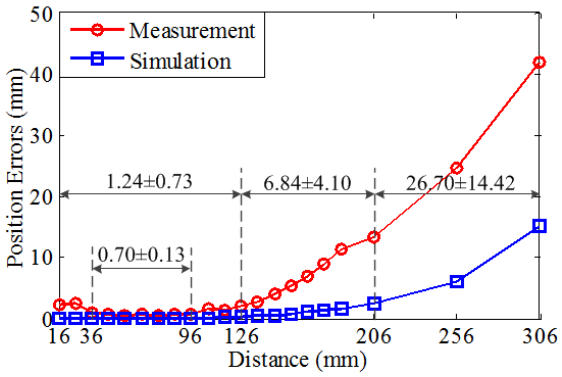

Fig. 12. Plot of the position error versus the distance between the sensor array and the magnet. *Measurement* means the measured position error of the magnetic tracking system, while *simulation* represents the simulation results when the noise is ±0.2uT at each axis.

and the sensor array. Fig. 11 shows the magnetic tracking system when the magnet was placed at the distance of 306mm.

Fig. 12 and Fig. 13 show respectively the location and orientation errors along with the distance in the range of 306mm. In addition, the simulation results with noise (±0.2uT in each axis) were added to Fig. 12 and Fig. 13.

As the red line in Fig. 12 and Fig. 13 shows, the average localization and orientation errors were 1.24 ± 0.74mm and $1.60 \pm 0.58°$ respectively when the magnet was placed from 16mm to 126mm above the sensor array. When the magnet located at the height from 36mm to 96mm above the sensor array, the system had the best performance, which average localization and orientation errors were 0.70 ± 0.13mm and $1.22 \pm 0.32°$ respectively.

The position error increased along with the distance when it was more than 106mm. The localization and orientation errors were bigger than 6.84mm and 5.97° respectively when the magnet was placed at the distance from 126mm to

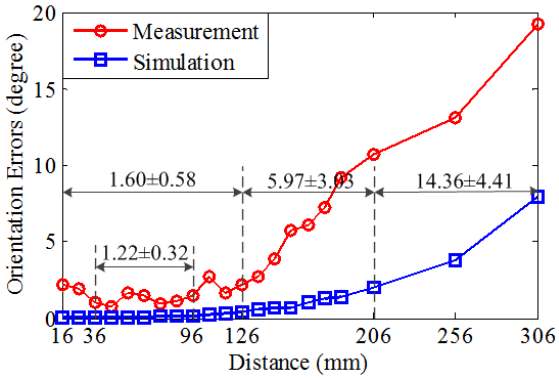

Fig. 13. Plot of the orientation error versus the distance between the sensor array and the magnet. *Measurement* means the measured orientation error of the magnetic tracking system, while *simulation* represents the simulation results when the noise is ±0.2uT at each axis.

206mm above the sensor array. In the experiment, the average localization and orientation errors were (13.34mm, 10.73°), (24.77mm, 13.09°), and (41.98mm, 19.27°) respectively when the magnet was placed at the distance of 206mm, 256mm, and 306mm.

According to the simulation results shown in Fig. 9 and Fig. 10, the primary reason for this tendency of the tracking accuracy along with the distance is that the signal-to-noise ratio (SNR) of the sensor array outputs were decreased along with the distance.

Especially, the simulation results were different to the experimental results for the distance from 16mm to 36mm, which denotes the tracking accuracy deteriorated when the magnet was too close to the sensor array. The reason is that the reduction of the number of effective sensors has little influence on tracking errors in simulation when there are more than two valid tri-axis sensors. At the distance of 30mm, B_{5z} was ±600uT, which exceeds the full scale of the magnetic sensors. Because the magnetic induction intensity was bigger than the range of the sensor, the valid sensors were reduced after the sensors with invalid data being disregarded.

Secondly, some simulations were performed to investigate the influences of sensor noise level and the magnet property to the tracking accuracies.

One primary difference between the experiments and simulations was the noise level, which resulted in the difference of position and orientation errors. Thus, simulations for N35 magnet, with different noise levels were carried out to investigate its effect on the tracking performance. The results are shown in Fig. 14 and Fig. 15.

As shown in Fig. 14 and Fig. 15, the simulated tracking accuracy decreased rapidly along with the distance between the sensor array and the magnet. We can find that the noise level had a significant influence when the distance was more than 100mm. Compared with the simulations of N35 with the varied noise level, it is clearly that the noise level affects the descent speed of the tracking accuracy.

Generally speaking, the higher grade of material, the stronger magnetic induction intensity of the magnet. The simulation of a grade N52 magnet (Ø10 × 10mm,

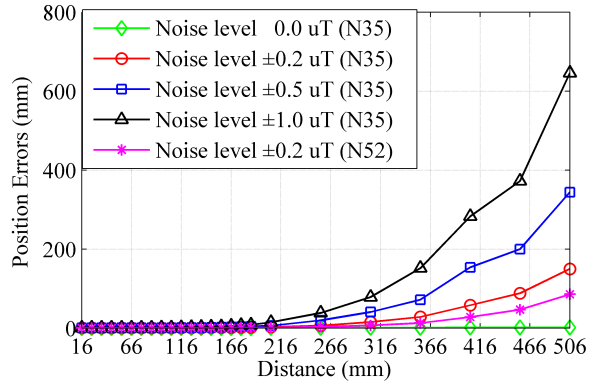

Fig. 14. Plot of the position error versus the distance between the sensor array and the N35 magnet. The noise level at each sensor axis of the sensor array varied from 0 to±1.0uT uT. In addition, the simulation based on a N52 magnet and the sensor noise level at ±0.2uT was added.

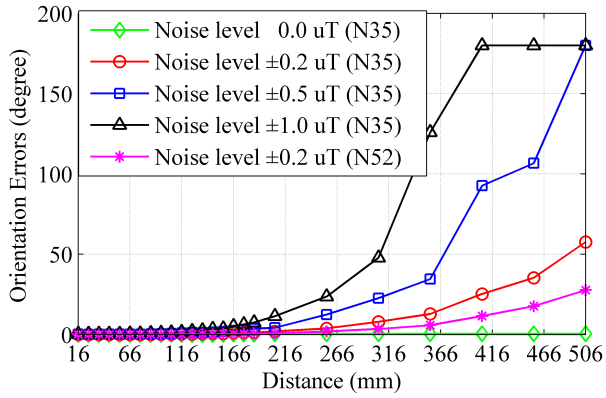

Fig. 15. Plot of the orientation error versus the distance between the sensor array and the N35 magnet.

$Br = 1.47 \pm 0.01$T), which has a bigger remanence than grade N35 (Ø10 × 10mm, $Br = 1.22 \pm 0.01$T), is also performed and displayed in Fig. 14 and Fig. 15. In addition, the simulation without noise for N35 was carried out. The comparison of all these results can be displayed in Fig. 14 and Fig. 15.

C. Regression Analysis for Accuracy-Versus-Distance

To investigate the quantitative relationship between the tracking accuracy and distance, regression analysis was performed with the curve fitting toolbox in Matlab R2014a (MathWorks Inc., USA) [26]. After comparison of Gaussian function, e-function, and polynomial function, a custom equation fitting, with the equation $f(x) = a_0 + a_1 x^b$, was chosen for regression because of its simple function form and a better fitting performance. Table II shows the adjusted r^2 values for the fittings of both position and orientation tracking, while Fig. 16 and Fig. 17 show the polynomial regression plots.

According to Table II and Fig. 16, the tracking accuracy decreased nonlinearly with the distance between the sensor array and the magnet, and its attenuation speed related to the properties of the magnet and SNR of the sensor outputs. Same to (18), the fitting function for position tracking tended to a polynomial of degree three.

TABLE II

PARAMETERS OF CUSTOM EQUATION FOR THE ACCURACY-VERSUS-DISTANCE RELATIONSHIP REGRESSION

	Adj-r^2, RMSE (position; orientation)	**Parameters** (position; orientation)
Measurement (N35)	0.9906,1.02 ; 0.9564, 1.07	a_0=0.274, a_1=1.251e-06, b=3.028; a_0=-0.686, a_1=9.229e-05, b=2.139
Simulation with noise (N35)	0.9832, 0.14; 0.9944, 0.10	a_0=-0.435, a_1=1.344e-07, b=3.218; a_0=-0.088, a_1=3.118e-07, b=2.966
Simulation with noise (N52)	0.9908, 0.08; 0.9602, 0.06	a_0=-0.092, a_1=5.689e-09, b=3.656; a_0=-0.135, a_1=1.956e-06, b=2.525

In this custom equation fitting, *f(x)* represents the tracking accuracy, while x means the tracking distance, a_0, a_1, and b are the regression coefficients. The noise level of each axis in the simulation with noise was ±0.2uT. Adj-r^2 (adjusted r^2) denotes the degree-of-freedom adjusted coefficient of determination. *RMSE* (root mean squared error) is also known as the fit standard error and the standard error of the regression.

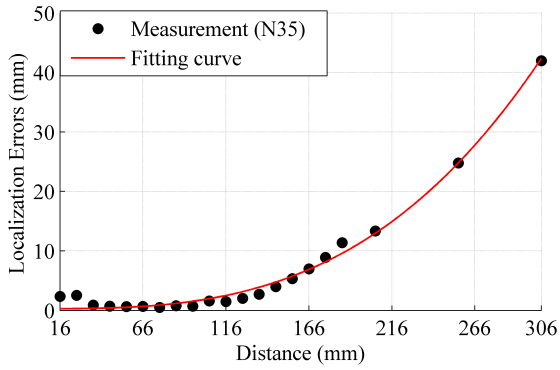

Fig. 16. Custom equation regression plot of the localization error versus the distance between the sensor array and the N35 magnet.

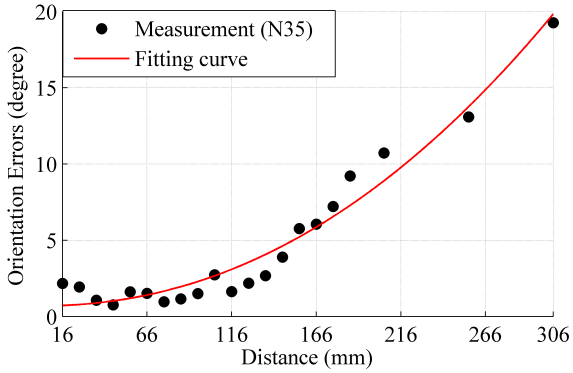

Fig. 17. Custom equation regression plot of the orientation error versus the distance between the sensor array and the N35 magnet.

D. Valid Tracking Distance Versus Remanence Br

Generally speaking, the higher the magnet grade, the higher the remanence *Br* and the stronger the magnetic induction intensity around the magnet. The above accuracy-versus-distance experiment was based on the N35 magnet. For a magnet with another grade, the tracking error-versus-distance relationships are different. According to the simulations of N35 and N52 magnets, we can see that the tracking errors along with distance increased more slowly with the distance

if the magnet was intensively magnetized. It is obvious that N52-based tracking has a bigger tracking distance compared with N35-based tracking.

According to (18) and Fig. 9, there is a varied tracking distance difference for these two types of magnets when the 5th sensor has the same B_{5z} or SNR value. The tracking distance difference (Δc) for a certain tracking accuracy between these two magnet grades can be acquired via (18):

$$B_{5z} = 2B_{T_N52}/c_{N52}^3 = 2B_{T_N35}/c_{N35}^3, \quad (19)$$

$$\Delta c = c_{N52} - c_{N35} = c_{N35}(\sqrt[3]{B_{T_N52}/B_{T_N35}} - 1). \quad (20)$$

For the magnet grade other than N52, (20) is also valid while B_{T_N52} and c_{N52} are replace by its related values.

When the magnet is not placed along with the Z-axis, $2B_T/c^3$ is the vector sum of magnetic field intensities in X-Y-Z- axes, other than in a single axis. According to Fig. 5, the tracking accuracy had small variation (<5%) when the magnet was placed in different points of the calibration board. Thus, (20) can be adapted for most situations.

VI. Conclusion

To analyze the relationship between the tracking accuracy and the distance from the magnet to the sensor array, a portable magnetic tracking system was built up based on the digital magnetic sensors in this study. The system structure is simplified, while it has low power consumption and convenient configuration via the SPI bus. After that, a series of simulations and experiments were carried out. The average localization error and orientation error at a distance from 36mm to 96mm above the sensor array are about 0.70mm and 1.22° respectively. The localization error rapidly increases with the distance when it was more than 106mm and reaches 40mm at the distance of 306mm.

In the following work, we will enlarge tracking space and achieve 6D tracking with the fusion of additional inertial sensing. Also, an embedded system (ARM or FPGA) will be adopted to perform the hybrid algorithm and to send the tracking results to other devices wirelessly. After further validation, this system will be utilized in the medical and industrial applications.

References

[1] J. Park, K. Jung, J. Kim, and S. Kim, "Accuracy improvement of magnetic guidance sensor using fuzzy inference system," in *Proc. Joint Int. Conf. Soft Comput. Intell. Syst.*, 2012, pp. 1639–1642.

[2] Y. Yu, L. Guo, M. Yang, and G. Zhu, "Graph-based SLAM based magnet map generation for magnetic guidance," in *Proc. IEEE Int. Conf. Robot. Biomimetics*, Dec. 2015, pp. 2661–2666.

[3] H. Cho, J. Kim, H. Song, M. Park, and S. Kim, "Method and development of magnetic positioning device for magnetic guided vehicle," in *Proc. Int. Conf. Intell. Robot. Appl.*, 2013, pp. 615–624.

[4] T. D. Than, G. Alici, H. Zhou, and W. Li, "A review of localization systems for robotic endoscopic capsules," *IEEE Trans. Biomed. Eng.*, vol. 59, no. 9, pp. 2387–2399, Sep. 2012.

[5] T. D. Than *et al.*, "An effective localization method for robotic endoscopic capsules using multiple positron emission markers," *IEEE Trans. Robot.*, vol. 30, no. 5, pp. 1174–1186, Oct. 2014.

[6] D. Son, S. Yim, and M. Sitti, "A 5-D localization method for a magnetically manipulated untethered robot using a 2-D array of Hall-effect sensors," *IEEE/ASME Trans. Mechatronics*, vol. 21, no. 2, pp. 708–716, Apr. 2016.

[7] C. D. Natali, M. Beccani, N. Simaan, and P. Valdastri, "Jacobian-based iterative method for magnetic localization in robotic capsule endoscopy," *IEEE Trans. Robot.*, vol. 32, no. 2, pp. 327–328, Apr. 2016.

[8] V. Schlageter, P.-A. Besse, R. S. Popovic, and P. Kucera, "Tracking system with five degrees of freedom using a 2D-array of Hall sensors and a permanent magnet," *Sens. Actuators A, Phys.*, vol. 92, nos. 1–3, pp. 37–42, 2001.

[9] V. Schlageter, P. Drljaca, R. S. Popovic, and P. Kučera, "A magnetic tracking system based on highly sensitive integrated Hall sensors," *Int. J. Ser. C Mech. Syst., Mach. Elements Manuf.*, vol. 45, no. 4, pp. 967–973, 2002.

[10] E. Stathopoulos, V. Schlageter, B. Meyrat, Y. de Ribaupierre, and P. Kucera, "Magnetic pill tracking: A novel non-invasive tool for investigation of human digestive motility," *Neurogastroenterol. Motility*, vol. 17, no. 1, pp. 54–148, 2005.

[11] J. T. Sherman, J. K. Lubkert, R. S. Popovic, and M. R. DiSilvestro, "Characterization of a novel magnetic tracking system," *IEEE Trans. Magn.*, vol. 43, no. 6, pp. 2725–2727, Jun. 2007.

[12] Y. Barrell and H. W. L. Naus, "Detection and localisation of magnetic objects," *IET Sci., Meas. Technol.*, vol. 1, no. 5, pp. 245–254, Sep. 2007.

[13] N. Wahlstro?m, J. Callmer, and F. Gustafsson, "Magnetometers for tracking metallic targets," in *Proc. Inf. Fusion*, 2010, pp. 1–8.

[14] C. Hu, M. Li, S. Song, W. Yang, R. Zhang, and M. Q.-H. Meng, "A cubic 3-axis magnetic sensor array for wirelessly tracking magnet position and orientation," *IEEE Sensors J.*, vol. 10, no. 5, pp. 903–913, May 2010.

[15] C. Hu, Y. Ren, X. You, and W. Yang, "Locating intra-body capsule object by three magnet sensing system," *IEEE Sensors J.*, vol. 16, no. 13, pp. 5167–5176, Jul. 2016.

[16] E. Paperno, I. Sasada, and E. Leonovich, "A new method for magnetic position and orientation tracking," *IEEE Trans. Magn.*, vol. 37, no. 4, pp. 1938–1940, Jul. 2001.

[17] C. Hu, S. Song, X. Wang, and Q. H. Meng, "A novel positioning and orientation system based on three-axis magnetic coils," *IEEE Trans. Magn.*, vol. 48, no. 7, pp. 2211–2219, Jul. 2012.

[18] X. Guo, C. Song, and R. Yan, "Optimization of multilayer cylindrical coils in a wireless localization system to track a capsule-shaped microdevice," *Measurement*, vol. 46, pp. 117–124, Jan. 2013.

[19] S. Song, C. Hu, B. Li, X. Li, and M. Q.-H. Meng, "An electromagnetic localization and orientation method based on rotating magnetic dipole," *IEEE Trans. Magn.*, vol. 49, no. 3, pp. 1274–1277, Mar. 2013.

[20] S. Song, X. Qiu, J. Wang, and Q. H. Meng, "Design and optimization strategy of sensor array layout for magnetic localization system," *IEEE Sensors J.*, vol. 17, no. 6, pp. 1849–1857, Mar. 2017.

[21] C. Hu, Q. H. Meng, M. Mandal, and X. Wang, "3-axis magnetic sensor array system for tracking magnet's position and orientation," in *Proc. 6th World Congr. Intell. Control Autom. (WCICA)*, 2006, pp. 5304–5308.

[22] C. Hu, Q. H. Meng, and M. Mandal, "The calibration of 3-axis magnetic sensor array system for tracking wireless capsule endoscope," in *Proc. IEEE/RSJ Int. Conf. Intell. Robots Syst.*, Oct. 2006, pp. 162–167.

[23] C. Hu, M. Q. Meng, and M. Mandal, "Efficient magnetic localization and orientation technique for capsule endoscopy," *Int. J. Inf. Acquisition*, vol. 2, pp. 23–36, Mar. 2005.

[24] W. Yang, C. Hu, M. Li, M. Q.-H. Meng, and S. Song, "A new tracking system for three magnetic objectives," *IEEE Trans. Magn.*, vol. 46, no. 12, pp. 4023–4029, Dec. 2010.

[25] M. Li, S. Song, C. Hu, W. Yang, L. Wang, and M. Q. H. Meng, "A new calibration method for magnetic sensor array for tracking capsule endoscope," in *Proc. IEEE Int. Conf. Robot. Biomimetics*, Dec. 2009, pp. 1561–1566.

[26] *Curve Fitting Toolbox User's Guide (Online)*, MathWorks, Natick, CA, USA, Mar. 2017, pp. 55–58.

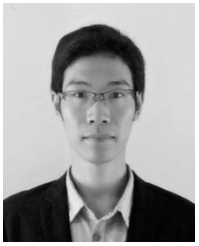

Shijian Su received the B.S. and M.S. degrees in electronic science and technology from the Fuzhou University, in 2012 and 2015, respectively. He is currently an Assistant Engineer with the Quanzhou Institute of Equipment Manufacturing, Haixi Institutes, Chinese Academy of Sciences, Quanzhou, China. His main research interests include intelligent sensors and magnetic localization.

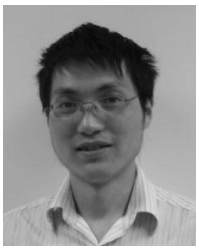

Wanan Yang received the M.S. degree from the Southwest Petroleum Institute in 2005 and the Ph.D. degree from the Chinese Academy of Sciences in 2011. He is currently a Professor with the School of Computer and Information Engineering, Yibin University, China. His main research areas include medical robotics, magnetic localization.

Houde Dai received the B.Eng. degree in biomedical engineering from the University of South China, Hengyang, China, in 2005, the M.S. degree in biomedical engineering from Tongji University, Shanghai, China, in 2009, and the Ph.D. degree in mechanical engineering from TU Munchen, Germany, in 2014. He is currently a Professor with the Quanzhou Institute of Equipment Manufacturing, Haixi Institutes, Chinese Academy of Sciences, Quanzhou, China. His research interests include intelligent sensors, information processing, and mobile robots.

Xuke Xia received the M.S. degree in electronic information engineering from the Anhui University of Science and Technology in 2015. He is currently an Assistant Engineer with the Quanzhou Institute of Equipment Manufacturing, Haixi Institutes, Chinese Academy of Sciences, Quanzhou, China.

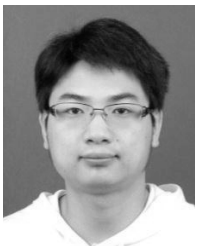

Mingqiang Lin received the B.S. and Ph.D. degrees in control science and engineering from the University of Science and Technology of China. He is currently with the Quanzhou Institute of Equipment Manufacturing, Haixi Institutes, Chinese Academy of Sciences, Quanzhou, China. His current research interests include computer vision, pattern recognition, and analysis and control of complex systems.

Bo Sun received the B.Eng. degree in biomedical engineering and the M.S. degree in control science and engineering from Shandong University, Jinan, China, in 2007 and 2011, respectively, and the Ph.D. degree in computer science and engineering from the University of Hamburg, Germany. He is currently a Senior Engineer with the Quanzhou Institute of Equipment Manufacturing, Haixi Institutes, Chinese Academy of Sciences, Quanzhou, China. His current research interests include computer vision, pattern recognition, and mobile robotic localization and navigation.

Chao Hu received the B.S. degree in electrical engineering and the M.S. degree in optical engineering from Zhejiang University, Zhejiang, China, in 1982 and 1986, respectively, and the Ph.D. degree in ECE from the University of Alberta, Canada, in 2006. He was a Research Professor with the Shenzhen Institute of Advanced Technology, CAS, from 2006 to 2011. He is a Professor and the Vice Dean of Information Science and Engineering with the Ningbo Institute of Technology, Zhejiang University. His primary research interests are in the areas of intelligent sensors, computer vision, medical electronics, and intelligent localization systems.